International Journal of Control, Automation and Systems 17(9) (2019) 2388-2399
http://dx.doi.org/10.1007/s12555-018-0327-z
ISSN:1598-6446 eISSN:2005-4092
http://www.springer.com/12555

A SLIP-based Robot Leg for Decoupled Spring-like Behavior: Design and Evaluation

Jaehong Seo, Jungyeong Kim, Sangshin Park, and Jungsan Cho*

Abstract: We present a spring loaded inverted pendulum (SLIP) based robot leg to enable decoupled swing motion and spring-like behavior. The two SLIP principles (decoupled swing motion and spring-like behavior) allow an improved understanding of robot locomotion and its control. Proposed leg mechanism include one degree of freedom (DOF) straight-line generating mechanism to perform ideal spring-like behavior and the pantograph to amplify that. The spring-like behavior can be implemented using mechanical constraints with Chebyshev linkage and the virtual spring method. For applying the virtual spring method to the radial motion controlled by one actuator, the relationship between the actuator force and radial force acting on the foot end was determined by using a kinematic interpretation. A 1-DOF test bed including the suggested leg was built and tested to verify the decoupled motions. The spring-like leg behavior was demonstrated during the free fall experiment and the experiment in which external force was applied.

Keywords: Biarticular leg, mechanism design, quadruped robot, SLIP, virtual stiffness.

1. INTRODUCTION

Most terrestrial animals, including humans, use appendages to stand on the ground, and can perform dynamic motions such as moving forward, running, or jumping using their limbs. Robots that use legs similar to those of ambulatory animals are called walking robots, and can have two legs like a human, four legs like a horse, or multiple legs like a spider. A larger number of legs allow static but stable walking, whereas a smaller number lead to more dynamic walking [1-3]. The wheels or caterpillar tracks used by most means of transport today provide limited mobility. Although a caterpillar track can advance over uneven terrain or raised spots, its motion limits it from accessing rugged mountains or climbing ladders. Many researchers are studying walking robots because their rough terrain adaptability can be useful in extreme tasks such as military operations or disaster assistance. The quadruped robots of Boston Dynamics, representatively, exhibit outstanding mobility and load capacity [4, 5].

The dynamic walking of a human or animal can be expressed as a center of mass (CoM) behavior, so a spring-loaded inverted pendulum (SLIP) is commonly used as a mathematical model [6-8]. A SLIP is a model composed of massless springs connected using revolute joints placed on the CoM and a point mass with the total mass. The running states of the SLIP are divided into the flight phase and the stance phase, which are differentiated by whether the foot is touching or leaving the ground [9-11]. In the

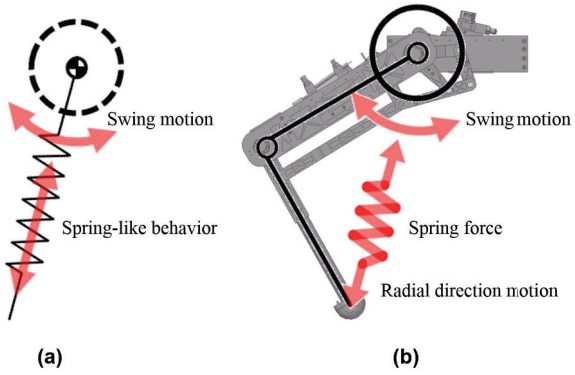

Fig. 1. Concept of a SLIP-based robot leg: (a) two principles of SLIP; a swing motion in the angular direction and spring-like behavior in the radial direction., (b) concept of the SLIP-based leg mechanism.

Manuscript received May 15, 2018; revised October 24, 2018 and April 5, 2019; accepted April 22, 2019. Recommended by Associate Editor Pilwon Hur under the direction of Editor Won-jong Kim. This work was supported by the Industrial Strategic technology development, 10047635, Development of Hydraulic Robot Control Technology based on Accurate and Fast Force Control for Complex Tasks funded by the Ministry of Trad, Industry & Energy (MI, Korea) .

Jaehong Seo and Jungyeong Kim are Ph.D candidates in Robotics and Virtual Engineering, University of Science and Technology, 217, Gajeong-ro, Yuseong-gu, Daejeon, Korea (e-mails: {jh_seo88, kjy880527}@kitech.re.kr). Sangshin Park and Jungsan Cho are with the Department of Robotics, Korea Institute of Industrial Techonology(KITECH), 143 Hangaul-ro, Sangnok-gu, Ansan-si, Korea (e-mails: {pss, chojs}@kitech.re.kr).
* Corresponding author.

flight phase of the SLIP, the feet are off the surface. The CoM draws a parabola that is dependent on the lift-off velocity. In the stance phase, the feet are on the surface. In the case of animals, the leg muscles contract, store energy, and then release it. The straight motion of the CoM and the energy storage/release could be expressed by a spring. Every movement of an SLIP, including these two phases, can be expressed by combining the principles of swing motion and spring-like behavior in Fig. 1. In the swing motion, the spring rotates centered on the CoM, whereas in the spring-like behavior, the spring enters a state of compression/relaxation.

SLIP-based walking presents self-stabilizing characteristic and high energy efficiency by utilizing its own and natural dynamics. However, ZMP-based walking of inverted pendulum(IP), which is the generally used method in bipedal robotics, cancels the natural dynamics of the robot. Because of these features, research on SLIP-based walking have been conducted using various methods.

The simplest way to realize a SLIP-based robot leg is to use linear actuators for the leg itself. Raibert realized one-, two-, and four-legged robots with telescopic legs [12]. As the most direct method of realizing a SLIP for a robotic platform, such a design accurately reflects the kinematic characteristics of a SLIP. However, in this case, the rod of the linear hydraulic actuator becomes the distal limb of the robot, which constantly collides with the ground. Therefore, the durability and range of motion (ROM) are limited. Most walking robots, for these reasons, are designed to implement SLIP motions and movements by using either an algorithmic or hybrid method. The latter involves employing a structure with a passive joint by using an actual spring to supplement the algorithmic method.

HyQ [13], was designed by the Italian Institute of Technology (IIT) and has a typical articulated leg with precise torque controlled joints. The revolute joints are operated by combining a linear hydraulic actuator and four-bar mechanism, where each abduction/adduction joint is operated by a rotary actuator. An advantage of this method is that the leg stiffness can be varied soft-ware-wise because the virtual spring that connects the hip joint and foot-end is realized by using precise joint torque control [14, 15].

The legs of BigDog (Boston Dynamics) and JINPOONG (KITECH) [16, 17] are also articulated like those of HyQ. Both robots have one redundant DOF (4 DOF per leg) and have actual springs at the distal limbs. This spring is why this approach is classified as a hybrid method. Because the spring functions as a mechanical low pass filter, it intuitively operates to regulate a repeated external force or large impact force as a passive component and guarantees an immediate response. Hence, the impact force created upon touchdown can be reduced with the spring of the distal joint, and the swing motions of the legs or body posture control can be implemented by combining the movements of the proximal joints. The spring used in the distal joint can be represented by the rotational joint stiffness from a biological perspective. Such legs designed with a more biological perspective include the segmented leg with knee spring [18-20]. This is another hybrid method for SLIP implementation. Although the use of actual springs increases the energy efficiency and reduces the impact force, vibration or chattering may occur during the stance phase. This disturbs the proximal joints, which negatively affects the stability of the robot's stance. A mechanism that conducts selective switching based on the status of the distal spring is sometimes used to solve this problem [21].

As described above, most of the robotic legs implement SLIP walking by using a serial structure that includes several links interconnected by revolute joints. These articulated legs, however, have a mechanical structure that is different from that of the SLIP model, and therefore the control approach should also be different. While the articulated leg controls multiple joint angles for end-effector position control, the SLIP model considers only the swing angle and the length of the radial direction. In this regard, Oh and Choi applied a biarticular actuation mechanism inspired by the human musculoskeletal system to achieve SLIP motion [22, 23].

Moreover, the articulated leg structure differs from SLIP not only in kinematic motion but also in the foot-end force control that generates the ground reaction force(GRF) during ground contact. A precise torque control of each joint is needed to produce a specific force (spring force) in a uniform direction (radial direction) on the foot-end for implementing SLIP without an actual spring. These joint torques can be calculated by using the Jacobian relationship between the task space and joint space. If the tracking performance of the desired torque given to each joint is not sufficient, the end-effector force is not uniform, and its motion cannot be kept straight. Especially when the revolute joint is driven by the combination of a linear hydraulic actuator and four-bar mechanism, precise and swift joint torque control is difficult because of the non-linearity and uncertainty of the hydraulic dynamics and the non-linearity between the actuator output force and joint torque. The slight wobbling motion due to the joint torque error creates issues in the stance phase when the feet of the robot are touching the ground. During trotting, when the robot has only two feet on the ground, this can cause disturbance torques to the body or move the CoM. Semini investigated the joint design in order to secure the linearity of joint torques and minimize the influence of such problems [24, 25].

To overcome such structural limits through the mechanical design method, we suggest a leg mechanism that includes a 1 DOF straight-line generating mechanism can perform a decoupled swing and radial motion. The straight-line generating linkage is a mechanism for producing a straight-line by combining several links and rev-

olute joints without any special guidance systems (e.g., linear motion guide, linear bushing, and slide). Since Watt invented the approximate straight-line generating mechanism for early steam engine designs in the late 18th century, the literature have been rich with various mechanical designs for straight-line motion. Various linkage mechanisms have been invented, including the Watt, Chebyshev, and Hoeckens linkages as approximate straight-line generating mechanisms and the Sarrus and Peaucellier linkages as exact straight-line generating mechanisms. Implementing a radial motion by using these linkage mechanisms guarantees the accuracy of the designed straight-motion and limits the straightness error to only the mechanical tolerance. It also allows to regard a knee flexion/extension as a simple 1 DOF motion, due to the radial motion that is operated by the 1 DOF linkage mechanism, instead of a combination of multiple joint motions. This is in contrast to articulated legs, which are also affected by the each joint torque control performance. Swing motions around the hip joint are also required; these can be induced by rotating the entire straight-line generating mechanism, around the hip joint.

This paper proposes a leg mechanism that can perform decoupled swing and radial motions by using a straight-line generating mechanism and pantograph. A kinematic analysis was performed to achieve the acquaintance with the suggested leg mechanism that differs from conventional articulated legs. The operational characteristics and kinematic relationship between the actuator force and foot-end force were analyzed to implement 1 DOF spring-like behavior, which was then verified experimentally. Section 2 describes the kinematic analysis of the suggested mechanism, which includes the forward kinematics and results of the kinematic simulation. Section 3 presents the relationship between the foot-end force and actuators and describes the virtual stiffness controller, which is derived from the force relationship. Section 4 explains how the robot leg was actually manufactured and describes how the characteristics were determined in an experiment with variable stiffness.

2. LEG DESIGN

2.1. Mechanism description

Motion generating mechanisms for particular purposes like the straight line generating mechanism in this study are usually used with a pantograph to amplify the generated motion. A pantograph is a structure comprising four links to form a parallelogram and is used to expand a structure by creating a specific movement because it can enlarge or reduce a point motion input by a specific ratio. Fig. 2(a) shows its structure. If the position of point O is fixed, the motion of point P is enlarged and copies the movements of point Q according to the linkage length ratio. Because most special paths or motion generating linkages have very complex shapes and are designed without considering durability (i.e., they are mostly designed in consideration of the generated motion), they are difficult to use as robot appendages. Hence, many studies have focused on utilizing pantographs with a relatively simple structure and the ability to enlarge, copy, and generate motions. Typical examples include the 1 DOF walking leg using a Chebyshev linkage [26, 27], the gravitationally decoupled actuation (GDA) using two actuators (although it is not a linkage mechanism) [28].

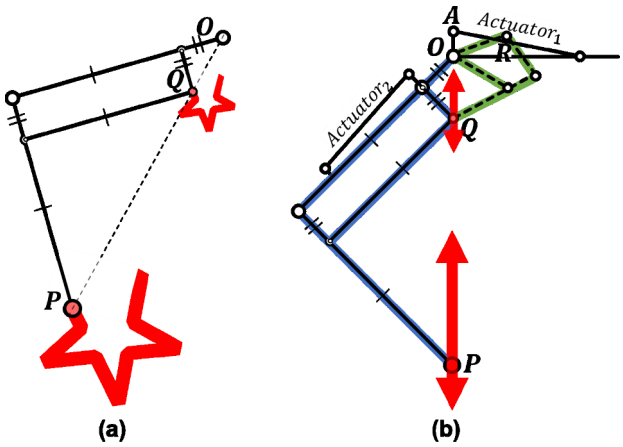

Fig. 2. Concept of the pantograph legs: (a) pantograph linkage feature amplifying the motion., (b) operating example for proposed leg mechanism; if $Actuator_1$ is fixed, line OA and OR also fixed, then a radial straight-line generated by $Actuator_2$.

Fig. 2(b) represents schematically assumed structure of the proposed robot leg that include a pantograph shaded blue and a 2-link motion generating linkage shaded green with dotted line. To create a mechanical 1 DOF radial motion with guaranteed straightness, the straight line generating mechanism based on the Chebyshev linkage was used in this study. In this case, the motions of the legs were limited by the 1 DOF movement of the four-bar linkage; hence, the radial motions can be created with another single actuator.

The operating process is as follows: If $Actuator_2$ is fixed, the entire leg, including the pantograph and Chebyshev linkage, becomes fixed and acts as one body. If $Actuator_1$ is activated in this state, all of the links below point O on the hip joint rotate equally centered on point O, which leads to a swing. On the other hand, if $Actuator_1$ is fixed, the line OR is fixed and acts as a ground link for Chebyshev linkage. If $Actuator_2$ is activated at this time, point Q draws a straight line along the line OP that connects the hip joint to the foot-end. Likewise, the swing motion operated by only $Actuator_1$ and the radial motion operated by only $Actuator_2$ are entirely independent of each other.

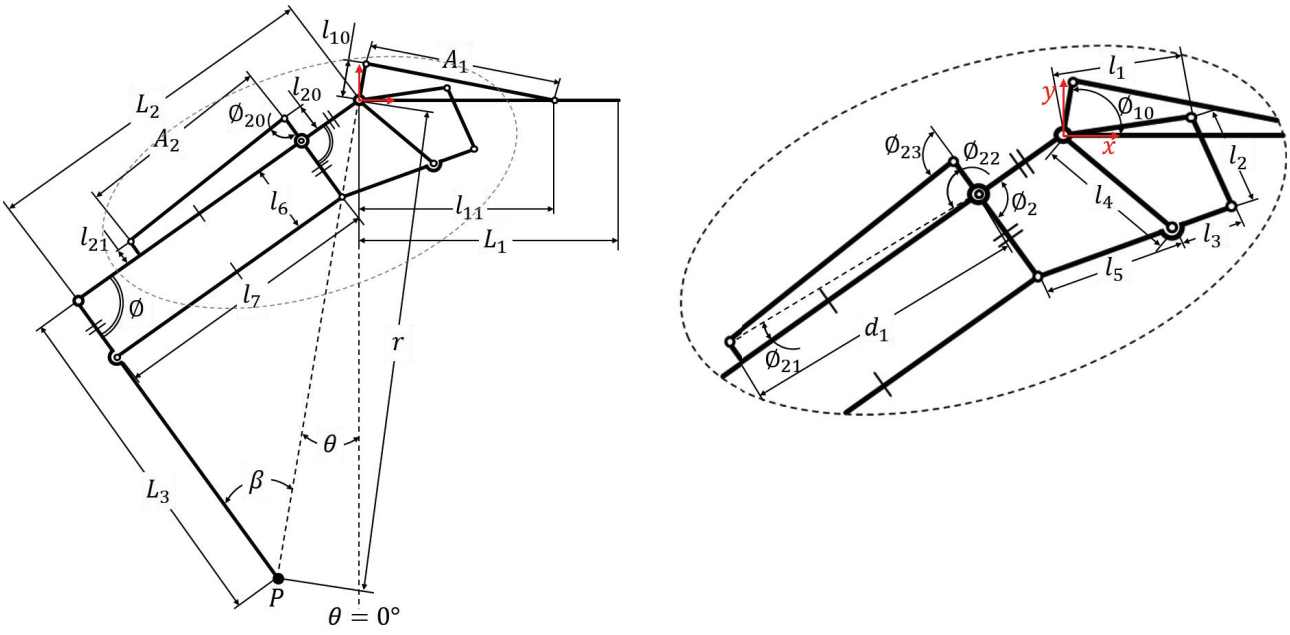

Fig. 3. Structure and dimensions of the suggested leg mechanism (left) and a zoomed-in view around the origin of the local coordinate frame (right).

2.2. Forward Kinematics

To determine the position of the robot's foot-end, we solve the forward kinematics for each actuator stroke. In the proposed mechanism, the foot-end position P can be calculated by

$$P = \begin{bmatrix} P_x \\ P_y \end{bmatrix} = \begin{bmatrix} r\sin\theta \\ -r\cos\theta \end{bmatrix}, \tag{1}$$

where r and θ are the length and angle of virtual leg, respectively (see Fig. 3). The symbols to denote the length of each link are presented in Table 1. The angle of virtual leg θ is

$$\theta = \frac{\pi}{2} - \phi_{10} \tag{2}$$

because link l_{10} and r are always collinear (see Fig. 3 (left)). In (2), ϕ_{10}, the angle between l_{10} and l_{11}, is determined by

$$\phi_{10} = \cos^{-1}\frac{{l_{10}}^2 + {l_{11}}^2 - {A_1}^2}{2l_{10}l_{11}}, \tag{3}$$

where A_1 represents the stroke of $Actuator_1$. The virtual leg length r can be calculated by

$$r = \sqrt{{L_2}^2 + {L_3}^2 - 2L_2L_3\cos\phi_{knee}}. \tag{4}$$

In (4), the knee angle ϕ_{knee} is equal to ϕ_2 due to the pantograph structure; from Fig. 3(right), ϕ_2, the angle between L_2 and l_{20}, is

$$\phi_2 = \phi_{21} + \phi_{22}, \tag{5}$$

in which ϕ_{22} can be obtained by

$$\phi_{22} = \cos^{-1}\frac{{d_1}^2 + {l_{20}}^2 - {A_2}^2}{2d_1l_{20}}, \tag{6}$$

where A_2 represents the stroke of $Actuator_2$. The values of d_1 and ϕ_{21} were 230 mm and 5 degree, respectively. These values were determined from the installed position of $Actuator_2$ and are not the variable of actuator stroke.

Table 1. Kinematic parameters of leg.

Link	Length [mm]	Link	Length [mm]
L_1	300	l_{20}	35
L_2	400	l_{21}	20
L_3	400	l_3	50
l_1	104	l_4	114
l_{10}	45	l_5	113
l_{11}	230	l_6	80
l_2	80	l_7	320

2.3. Kinematic simulation

Each of the linear actuators used for the leg had a stroke of 227 ± 27 mm. Fig. 4 shows the result when $Actuator_1$ and $Actuator_2$ were operated in combination. In the case of the swing motion, when only $Actuator_1$ was operated while the virtual line connecting the hip joint and foot-end was vertical, the hip joint had an operating range of

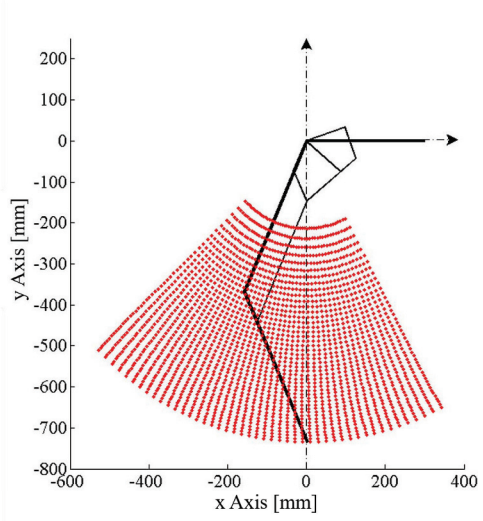

Fig. 4. Range of motion on the sagittal plane. It presents the foot-end position decomposed into the rotation angle about the hip joint and the leg length.

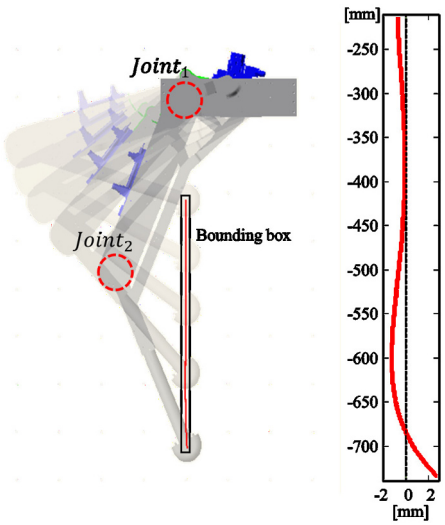

Fig. 5. Straightness of radial motion as obtained from simulation model.

-46° to $+27^\circ$. The radial motion had a radial leg length of 214-734 mm depending on the $Actuator_2$ stroke.

Fig. 4 also shows one of the main features of the suggested mechanism: maintaining the radial direction regardless of the swing angle. The suggested mechanism achieves a flexion/extension motion of the foot-end in the radial direction that is centered on the hip joint. Hence, the straightness ε of the radial motion can be taken as a performance index for the leg mechanism. Lipson used the concept of the bounding box to evaluate the straightness of a mechanism designed with genetic programming (GP) [29].

As shown in Fig. 5, the length over the width of the bounding box that tightens a particular path indicates the maximum deviation from an exactly straight line. When the straightness of the suggested mechanism was evaluated, the result was 1:128 (7.8125e-3). The straightness of the mechanism can be expressed by the equation below. This suggests that, for a motion of approximately 1000 mm, the maximum deviation from an absolutely straight line would be less than 4 mm.

$$\varepsilon = \frac{P_{x,max} - P_{x,min}}{P_{z,max} - P_{z,min}} = \frac{(\text{The Width of Bounding Box})}{(\text{The Height of Bounding Box})}.$$

3. VIRTUAL SPRING IMPLEMENTATION

3.1. Calculating the Foot-end Force

The most intuitive way to measure the foot-end force is to install a multi-axis load cell on the foot. However, this is not a general method because of the increasing leg inertia and repetitive collisions that might cause sensor malfunction. A more general method is calculating the foot-end force by using the Jacobian relationship between the foot-end and each joint.

The hip joint torque and radial force are determined by the input force of $Actuator_1$ and $Actuator_2$ as Fig. 6. These forces are denoted by τ_h, F_r, F_1 and F_2 respectively. First, the τ_h can be calculated form the F_1 and the effective lever arm ($l_{10,e}$) as follows:

$$\tau_h = l_{10,e} F_1. \tag{7}$$

In (7), $l_{10,e}$ can be calculated by

$$l_{10,e} = l_{10} \sin\phi_{11}, \tag{8}$$

in which ϕ_{11} can be obtained by

$$\phi_{11} = \cos^{-1} \frac{{A_1}^2 + {l_{10}}^2 - {l_{11}}^2}{2 A_1 l_{10}}. \tag{9}$$

Next, F_r can be derived from the force transmission relationship among the links (under the assumption that the leg is in static equilibrium). The relation between F_r and F_2 which can be obtained from force and moment equation under static equilibrium condition are derived as follows (You can see the derivation procedures of the at Appendix A):

$$F_r = \frac{l_{20} \sin\phi_{23}}{L_3 \sin\beta} F_2. \tag{10}$$

In (10), ϕ_{23} and β, denoted by the angle between $Actuator_2$ and link l_{20} and the angle between the L_3 and virtual leg respectively, can be calculated by

$$\phi_{23} = \pi - \phi_{20}, \tag{11}$$

$$\beta = \frac{\pi - \phi_2}{2}, \tag{12}$$

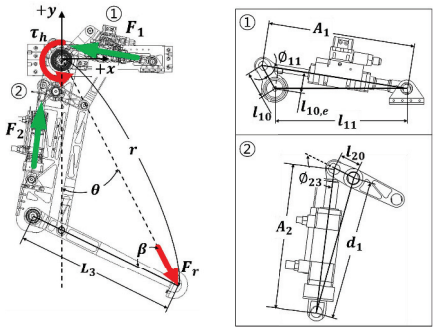

Fig. 6. Force relationship between input ($Actuator_1$, $Actuator_2$) and output (hip joint torque and radial force on the foot-end).

in which ϕ_{20} can be obtained by

$$\phi_{20} = \cos^{-1} \frac{{A_2}^2 + {l_{20}}^2 - {d_1}^2}{2A_2 l_{20}}. \tag{13}$$

Consequently, a foot-end force (F_{foot}) can be calculated with generalized forces $F_g = [\tau_h, F_r]^T$ using Jacobian transpose relationship.

$$F_{foot} = (J^T)^{-1} F_g \tag{14}$$

in which J can be obtained by

$$J = \begin{bmatrix} \sin\theta & r\cos\theta \\ -\cos\theta & r\sin\theta \end{bmatrix}. \tag{15}$$

3.2. Radial force simulation

The above relationship between the F_2 and F_r was validated by using the RecurDyn (FunctionBay, Inc., Korea) multibody dynamics simulator. As shown in Fig. 7, the simulation consisted of a block touching the foot-end and a connected spring to allow the block to move under the influence of the foot-end force. The hip joint position was fixed in space. $Actuator_1$ was fixed, and the radial motion was produced only by $Actuator_2$. Movement between the block and foot-end was only generated in the radial direction. The contact force resulting from this motion also acted in the radial direction. In short, because the contact force and radial force in this simulation were equal in magnitude but acted in opposite directions, it was possible to obtain the radial force. The radial force was calculated from the force F_2 and (10). The obtained value was almost identical to the simulation result (Fig. 7(b)).

3.3. Leg stiffness controller

As discussed in Section 3.1., the suggested mechanism can easily produce a radial force using only the force of $Actuator_2$. Conversely, the F_2 to produce the desired radial force can be obtained, and the virtual spring that connects the hip joint to the foot-end can be realized simply

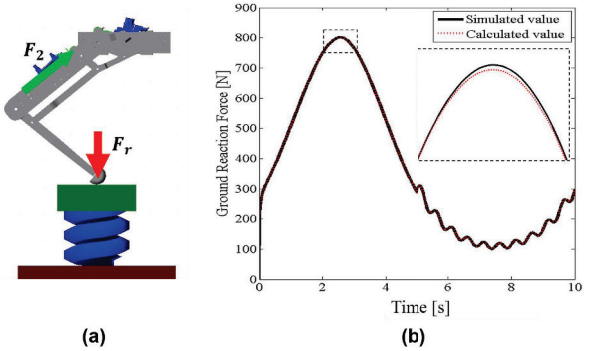

Fig. 7. Dynamic simulation model and the result: (a) model for verifying the force relationship between the force of $Actuator_2$ and the radial force, (b) comparison between the dynamic simulation and calculation by (10).

by controlling the F_2. The desired radial force was calculated by using a virtual spring damper model, as shown in Fig. 9.

$$F_r = k\Delta r + c\dot{r} \tag{16}$$

In the above equation, k and c represent the spring and damping coefficients, respectively, of the virtual components. r expresses the virtual leg length, which represents the distance between the hip joint and foot-end. If a high k is set, a rigid leg can be implemented like under position control; if it is set to be relatively low, a compliant characteristic can be implemented by generating a sufficient flexion when an external force is applied. For c, no specific value is provided by the controller. Individual joints friction, frictional force of the actuator,the elasticity of the hydraulic hose, etc. act as c; this will need to be compensated later.

4. EXPERIMENT

4.1. 1-DOF Test-bed

As discussed in Section II, the ROM of the leg was examined by using forward kinematics and a dynamic simulation. Fig. 8 shows each motion of the manufactured leg. The ROMs of the joint and each actuator of the leg were identical to the design. Fig. 8(b) also shows that the straightness of the radial motion was effectively maintained in the actual leg. The manufactured leg and the test bed with the linear motion guide (LM guide) were made of hardened anodized aluminum (AL6061-AHC) to minimize the weight. Each shaft was manufactured from bearing steel. While $\phi 12$ shafts were generally used, $\phi 15$ and $\phi 20$ shafts were used for parts that had to carry significant loads. The weight of the assembled leg, including all components such as the actuators and bearings, totaled about

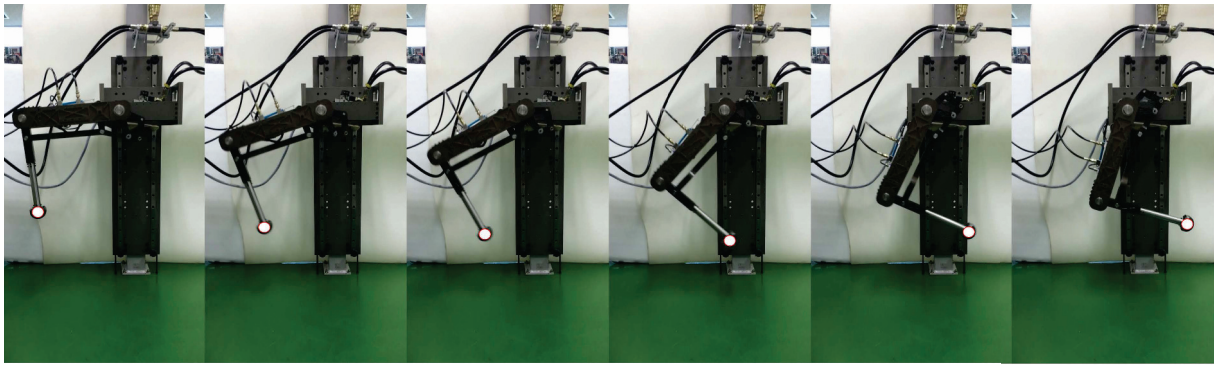

(a)

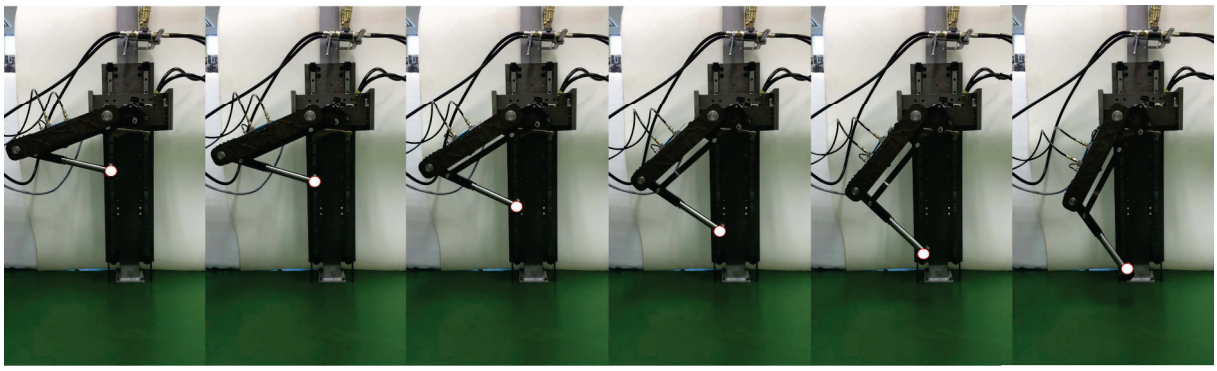

(b)

Fig. 8. Snapshot of each SLIP motion with graphically highlighted foot-end: (a) swing motion in the angular direction that is centered on the hip joint actuated by $Actuator_1$ and the (b) radial motion actuated by $Actuator_2$.

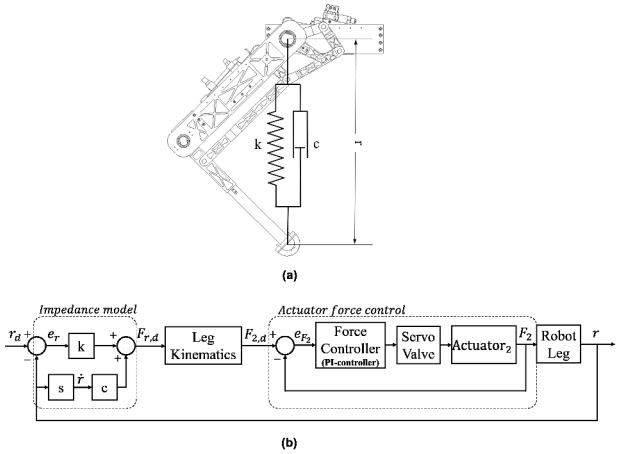

Fig. 9. (a) Reference model of the virtual spring connecting the hip joint and foot-end and the (b) block diagram for virtual stiffness controller; subscripts d denote the desired values and letter e_r, e_{F_2} denote error of leg length and force of $Actuator_2$, respectively.

17 kg. The weight of the carrier used to connect with the LM guide was about 3 kg. The LM guide limited the leg motion to 1 DOF. Thus, it was only capable of motion along the Z-axis. Because the abduction/adduction motion of the hip was excluded from the manufactured test bed, two linear actuators were used to produce the swing and radial motions. For the swing motion of hip joint, a double rod actuator (JP-10-54-M-SV, KNR Systems INC., Korea) of $\phi 28$ of piston diameter and $\phi 12$ of rod diameter was used. For the radial motion, a single rod actuator (KA-32, KITECH, Korea) of $\phi 32$ and $\phi 20$ of piston and rod diameter allows to withstand the payload of 900 N with 210 bar of supplied pressure. The flow of the actuator was determined by a flow control servo-valve (200-0035, Star Hydraulics Ltd., UK). The sensor system utilized a linear potentiometer (SLS095, Penny and Giles Controles Ltd., UK) to measure the actuator stroke for actuator control, a load cell(CDES-2T, Bongshin Loadcell Co., LTD., Korea) to measure the actuator force. The control system was executed by 1 kHz of control frequency with the UEISIM 300 (United Electronic Industries, USA) digital controller that equipped DAC and ADC (16 bits).

4.2. Discussion

Fig. 10(a) compares the theoretically calculated values for k at 800, 1200, and 1600 N/m and the experimental value obtained through implementation of the spring force. In this experiment, the spring force was measured

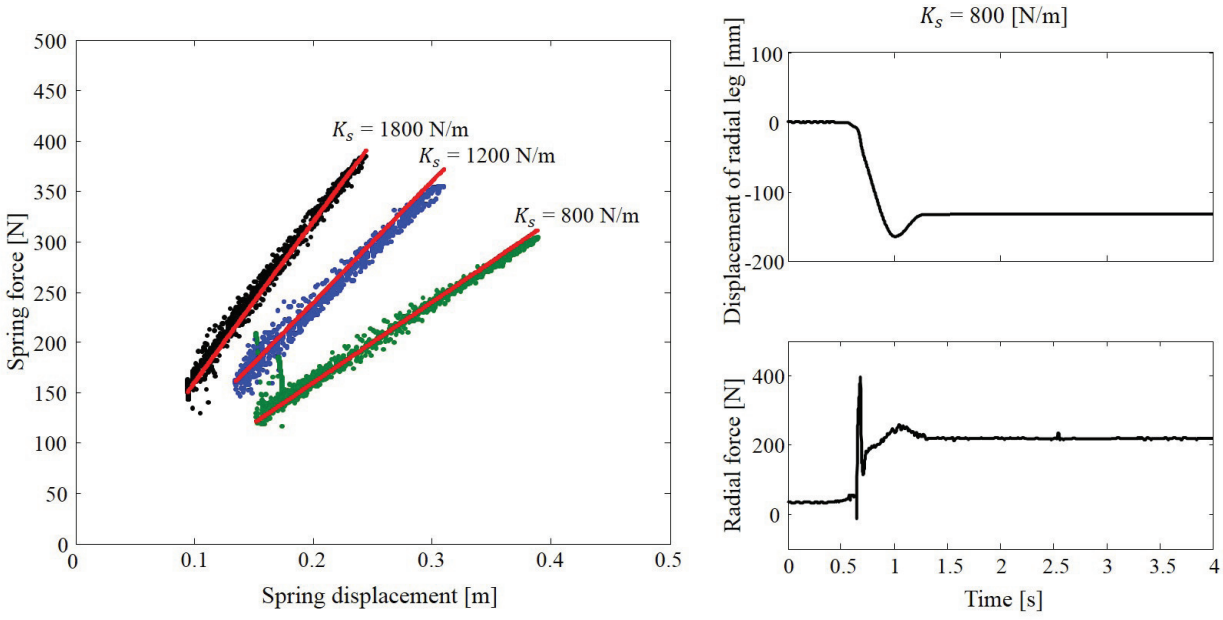

Fig. 10. Implementation results of a virtual spring: (a) verification of the actual stiffness; the result of compliance motion of the leg, which has variable stiffness, in contact with the ground, (b) results for a free-fall experiment; when free-falling, the leg experiences a virtual stiffness of 800N/m, the impact force, which is 2 times the total weight of the leg, occurs and cause bending of the knee.

while the spring displacement was changed by application of a vertical external force to each leg to realize a virtual spring. The virtual spring realized through the force control of the actuator showed results similar to the theoretical results.

Fig. 10(b) shows the displacement of the radial leg length and the radial force produced when the leg was dropped from a height of 0.2 m to realize a virtual spring of 800 N/m by controlling the force applied by $Actuator_2$. The radial force did not fall to zero, although the foot-end was not in contact with the ground (Fig. 10(b), before 0.6 s), according to the radial force calculated from the force applied by $Actuator_2$. The effects of the radial force during the flight phase can be eliminated by applying a method that distinguishes between the flight and stance phases. Fig. 11 shows that, when an external force is applied in the vertical direction to a leg standing at a certain height above the surface of the ground, the motion changes according to the properties of the virtual spring damper. When the virtual leg is set to a high stiffness, a small displacement of the radial leg and high radial force arise as a result of the external force. A low stiffness, on the other hand, results in more compliant movement and a reduction in the radial force as a result of the compliance. These results show that a virtual spring can be realized by controlling the force applied by $Actuator_2$ only. A variable stiffness can be realized by adjusting the characteristics of the virtual spring model.

Fig. 10 and Fig. 11 show the results of variable stiffness implementation and the limitation of impact force regulation. The jerky forces, which are a limitation of the feedback controller because it reacts only after impact, occur before and after the impact force. Although this problem can intensify during high speed running, it can be resolved by predicting ground contact and more precise force feedback control using a higher control frequency.

5. CONCLUSION

A SLIP-based leg was implemented that can decouple the swing motion and spring-like behavior of widely used SLIP mechanisms to interpret and plan the locomotion of a walking robot. This leg mechanism was designed to include a straight-line generating mechanism and pantograph in order to generate a straight radial motion and amplify it, respectively. Geometric methods were used to interpret the mechanism. The swing motion and spring-like behavior are not affected by each other, and the kinematic simulation showed that the straightness of the radial motion is mechanically guaranteed. A feature of the leg mechanism is that the spring force acting on the foot-end can be realized by controlling the force of only one actuator. This feature makes realizing the spring-like behavior of SLIP simple, unlike articulated legs that carry out the same task through collaborative force control of several actuators. The virtual and ideal spring properties were

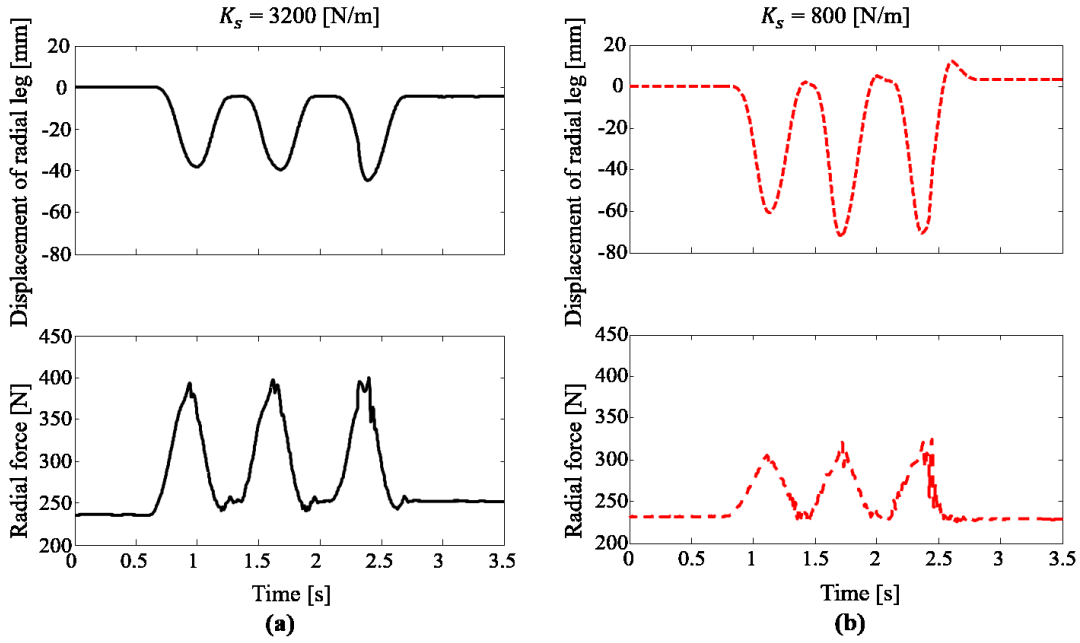

Fig. 11. Result of applying an external force to a leg at a certain height with variable stiffness; the radial force is seen to increase on application of an external force, and the leg length varies because of this radial force.

compared for several different stiffness values to demonstrate the possibility of implementing a variable stiffness. Based on these results, combining the decoupled mechanism and actuator force control can help regulate the impact force at touch-down and interaction with the ground surface for walking on uneven terrain. Future studies will use the proposed leg mechanism to address the complex effects of the radial force and swing torque during 2 DOF planar hopping, which is the basis of walking.

APPENDIX A

A.1. Proof of (10)

To derive the relation between input (F_2) and output forces (F_r) under static equilibrium, we should define the free body diagram of robot leg first. The free body diagram of whole proposed system is shown as Fig. A.1(a). However, the number of governing equations is only 3 while the needed number of unknown external forces is 5. So we should rewrite free body diagram (Fig A.1(b)) for each components. The total number of governing equations and unknown external/ internal forces are 21 equally. Although we can obtain all unknown external/internal forces, the whole calculation procedures of solutions are too complex and many iterations to obtain all solutions are needed. For the simplicity of the procedures and solutions, we assume the conditions of internal forces acting on point H as follows: The ground of upper assumption can be confirmed by the simulation result as shown Fig. A.2.

Assumption 1: The internal forces acting on point H of link HIJ is negligible.

Now, let derive the relation between F_G and F_2 using original and modified free body diagram under Assumption 1 (Fig. A.3). First, from observation at modified free body diagram 7‘ (Fig. A.3(a)), F_{ABH} can be derived as follows:

$$F_{ABH} = F_{EH}. \tag{A.1}$$

Next, from observation at modified free body diagram 8‘ (Fig. A.3(b)), the corresponding moment equation can be obtained as follows:

$$\sum M_B = 0: \tag{A.2}$$

$$-L_{AB}F_2\sin(\pi-\phi_{23}) + L_{BH}(F_{EH})_n = 0, \tag{A.3}$$

and $(F_{EH})_n$ can be derived from (A.2) as follows:

$$(F_{EH})_n = \frac{L_{AB}F_2\sin(\pi-\phi_{23})}{L_{BH}}. \tag{A.4}$$

Finally, from observation at free body diagram 11 (Fig. A.3(c)), the corresponding moment equation can be obtained as follows:

$$\sum M_D = 0: \tag{A.5}$$

$$L_{DG}F_G\sin(\beta) - L_{DE}(F_{EH})_n = 0, \tag{A.6}$$

and the relation between F_G and F_2 can be derived from (A.3) and (A.4) as follows:

$$F_G = \frac{L_{AB}\sin(\phi_{23})}{L_{DG}\sin(\beta)}F_2 \quad (\because L_{BH} = L_{DE}). \tag{A.7}$$

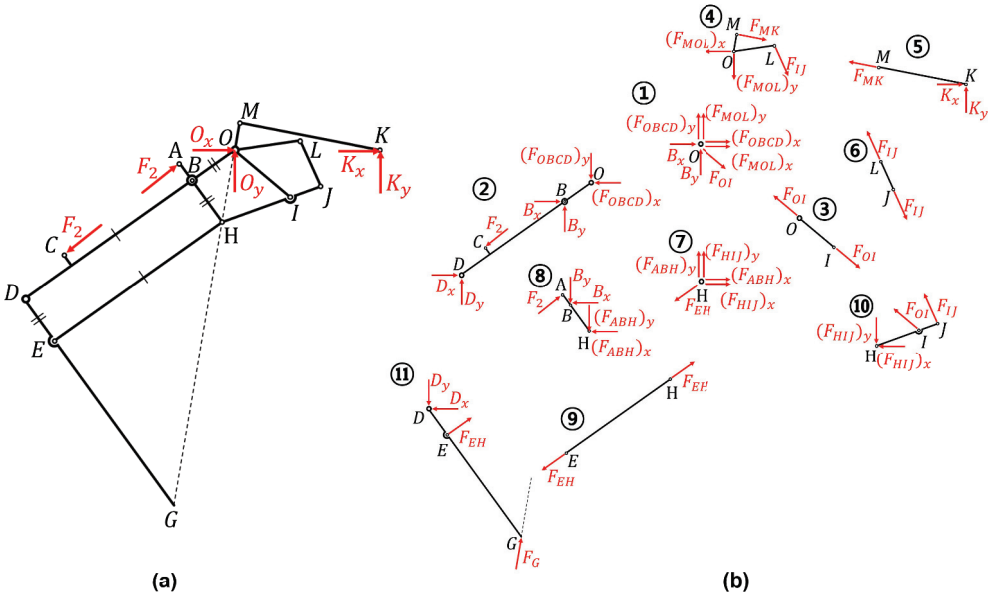

Fig. A.1. The free body diagram of proposed robot leg: (a) whole proposed system, (b) each components of proposed system.

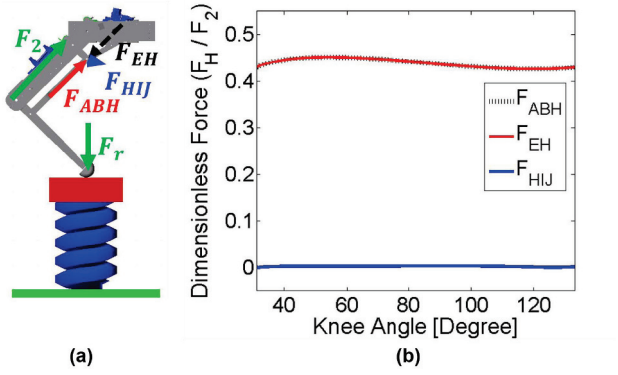

Fig. A.2. The simulation model for Assumption 1: (a) simulation model shows relationship between input and output force on the point H of the free body diagram across whole of the radial motion, (b) during quasi static motion, the force F_{ABH} and F_{EH} are present same tendency while (F_{HIJ}) is almost zero.

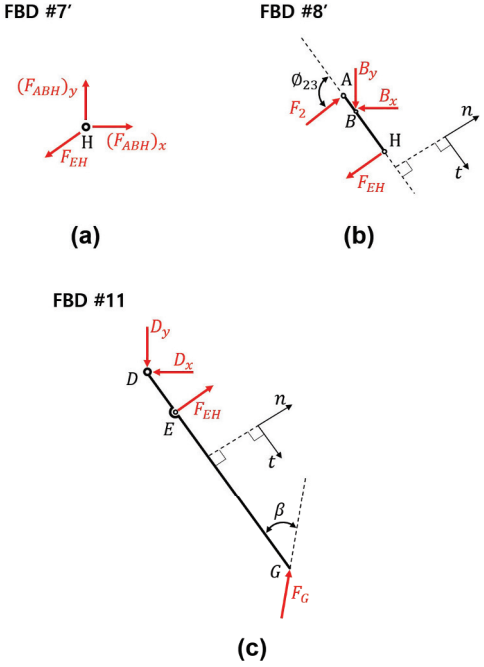

Fig. A.3. The original(#11) and modified(#7‘ and #8‘) free body diagram which are needed for obtaining the relation F_G and F_2 under Assumption 1.

Equation (A.5) can be rewrote with the notation of link length on this paper as follows:

$$F_G = \frac{l_{20}\sin(\phi_{23})}{L_3\sin(\beta)}F_2 \quad (\because l_{20} = L_{AB},\ L_3 = L_{DG}). \quad \text{(A.8)}$$

REFERENCES

[1] R. Blickhan and R. J. Full, “Similarity in multilegged locomotion: bouncing like a monopode,” *J. Comp. Physiol. A Neuroethol. Sens. Neural. Behav. Physiol.*, vol. 173, no. 5, pp. 509-517, 1993.

[2] L. H. Ting, R. Blickhan, and R. J. Full, “Dynamic and static stability in hexapedal runners,” *J. Exp. Biol.*, vol. 197, no. 1, pp. 251-269, 1994.

[3] J. Schmitt, M. Garcia, R. C. Razo, P. Holmes, and R. J. Full, "Dynamics and stability of legged locomotion in the horizontal plane: a test case using insects," *Biol. Cybern.*, vol. 86, no. 5, pp. 343-353, 2002.

[4] M. Raibert, K. Blankespoor, G. Nelson, R. Playter, and the BigDog Team, "BigDog, the rough-terrain quadruped robot," *Proc. of 17th IFAC World Congr.*, Seoul, Korea, pp. 10822-10825, 2008.

[5] D. V. Lee and A. A. Biewener, "BigDog-inspired studies in the locomotion of goats and dogs," *Integr. Comp. Biol.*, vol. 51, np. 1, pp. 190-202, July 2011.

[6] R. Blickhan, "The spring-mass model for running and hopping," *J. Biomech.*, vol. 22, no. 11, pp. 1217-1227, 1989.

[7] R. J. Full and D. E. Koditschek, "Templates and anchors: neuromechanical hypotheses of legged locomotion on land," *J. Exp. Biol.*, vol. 202, no. 23, pp. 3325-3332, 1999.

[8] R. Altendorfer, U. Saranli, H. Komsuoglu, D. E. Koditschek, H. B. Benjamin Brown, M. Buehler, E. Moore, D. McMordie, and R. Full,, "Evidence for spring loaded inverted pendulum running in a hexapod robot," *Experimental Robotics VII*, pp. 291-302, Springer, Berlin, 2001.

[9] O. Arslan, U. Saranli, and O. Morgul, "An approximate stance map of the spring mass hopper with gravity correction for nonsymmetric locomotions," *Proc. of IEEE ICRA*, Kobe, Japan, May, 2009.

[10] R. M. Alexander, "Three uses for springs in legged locomotion," *Int. J. Robot. Res.*, vol. 9, no. 2, pp. 53-61, 1990.

[11] I. Poulakakis and J. W. Grizzle, "The spring loaded inverted pendulum as the hybrid zero dynamics of an asymmetric hopper," *IEEE Trans. Autom. Control*, vol. 54, no. 8, pp. 1779-1793, 2009.

[12] M. H. Raibert, *Legged Robots that Balance*, MIT Press, Cambridge, 1986.

[13] C. Semini, *HyQ-Design and Development of a Hydraulically Actuated Quadruped Robot*, Ph.D. Dissertation, Univ. Genoa, Genoa, Italy 2010.

[14] I. Havoutis, C. Semini, J. Buchli, and D. G. Caldwell, "Quadrupedal trotting with active compliance," *Proc. of IEEE Int. Conf. Mechatronics*, Vicenza, Italy, 2013.

[15] M. Focchi, T. Boaventura, C. Senmini, M. Frigerio, J. Buchli, and D. G. Caldwell, "Torque-control based compliant actuation of a quadruped robot," *Proc. IEEE Int. Workshop Advanced Motion Control*, Sarajevo, Bosnia, 2012.

[16] J. Cho, J. T. Kim, S. Park, and Y. Lee, "JINPOONG, posture control for the external force," *Proc. IEEE Int. Symp. Robotics*, Seoul, Korea, Oct., 2013.

[17] J. Cho, J. T. Kim, S. Park, and K. Kim, "Dynamic walking of JINPOONG on the uneven terrain," *Proc. IEEE Int. Conf. Ubiquitous Robots and Ambient*, Jeju, Korea, 2013.

[18] H. Geyer, A. Seyfarth, and R. Blickhan, "Compliant leg behavior explains basic dynamics of walking and running," *Proc. R. Soc.*, 2006.

[19] N. Rao, Z. Shen, and J. Seipel, "Comparing legged locomotion with a sprung-knee and telescoping-spring when hip torque is applied," *Proc. IDETC/CIE: International Design Engineer Technical Conference*, Portland, Oregon, 2013.

[20] Z. G. Zhang, Y. Fukuoka, and H. Kimura, "Adaptive running of a quadruped robot using delayed feedback control," *Proc. IEEE int. conf. Robotics and Automation*, 2005.

[21] J. Cho, S. Park, and K. Kim, "Design of mechanical stiffness switch for hydraulic quadruped robot legs inspired by equine distal forelimb," *Electron. Lett.*, vol. 51, no. 1, pp. 33-35, 2014.

[22] S. Oh, K. Kong, "Realization of spring loaded inverted pendulum dynamics with a two-link manipulator based on the bio-inspired coordinate system," *Proc. IEEE int. conf. Robotics and Automation*, Hong Kong, China, 2014.

[23] H. Choi, S. Oh, and K. Kong, "Control of a robotic manipulator in the polar coordinate system using a biarticular actuation mechanism," *Int. J. Control. Autom.*, vol. 14, no. 4, pp. 1095-1105, 2016.

[24] C. Semini, N. G. Tsagarakis, B. Vanderborght, Y. Yang, and D. G. Caldwell, "HyQ-hydraulically actuated quadruped robot: hopping leg prototype," *Proc. IEEE Int. Conf. Biomedical Robotics and Biomechatronics*, Scottsdale, USA, 2008.

[25] H. Khan, R. Featherstone, D. G. Caldwell, and C. Semini, "Bio-inspired knee joint mechanism for a hydraulic quadruped robot," *Proc. IEEE int. conf. Robotics and Automation*, Seattle, USA, 2015.

[26] M. Couto, C. P. Santos, and J. Machado, "Modelling and design of a tridimensional compliant leg for bioloid quadruped," *J. Appl. Math. Inf. Sci.*, vol. 8, no. 4, pp. 1501-1507, 2014.

[27] C. Liang, M. Ceccarlli, and Y. Takeda, "Operation analysis a one-DOF pantograph leg mechanism," *Proc. of the RAAD*, pp. 15-17, 2008.

[28] K. Arikawa and S. Hirose, "Mechanical design of walking machines," *J. Philos. T. Roy. Soc. A*, vol. 365, no. 1850, pp. 171-183, 2007.

[29] H. Lipson, "How to draw a straight line using a GP: benchmarking evolutionary design against 19th century kinematic synthesis," *Proc. GECCO*, Seattle, USA, 2004.

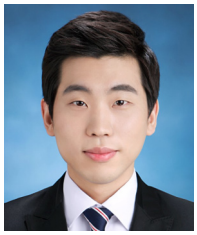

Jaehong Seo received his B.Eng. degree in Mechanical Engineering from Gachon University, Korea in 2014. He is currently a Ph.D. candidate in Robotics and Virtual Engineering at University of Science & Technology and also a researcher fellow in Department of Robotics, Korea Institute of Industrial Technology. His research interests include bio-inspired robot, hydraulic quadruped robot.

Jungyeong Kim received his B.Eng. degree in Mechanical Engineering from Konkuk University, Korea in 2012, and his M.Eng. degree in Robotics and Virtual Engineering from University of Science & Technology, Korea in 2016, where he is currently working toward a Ph.D. degree. He is also a researcher fellow in Department of Robotics, Korea Institute of Industrial Technology. His research interests include cable-driven mechanism, hydraulic manipulator, quadruped robot.

Sangshin Park received his B.Eng. and M.Eng. degrees in Electronic Engineering and Control and Embedded System from Kumoh National Institute of Technology, Korea, in 2009 and 2011, respectively. He is currently working at Department of Robotics, Korea Institute of Industrial Technology. His research interests include robot control, embedded system.

Jungsan Cho received his B.Eng. and M.Eng. degrees in Electronic Engineering from Kumoh National Institute of Technology, Korea, in 2002 and 2004, and the Ph.D. degree in Electronic Engineering from Myongji University, Korea in 2015. He is currently the Head of the Hydraulic Robot Research Laboratory at Korea Institute of Industrial Technology, and the Associate Professor at Robotics and Virtual Engineering, University of Science & Technology. His research interests include quadruped robot, hydraulic robot, hydraulic control.